



ORIGINAL ARTICLE

Enhanced thermal and tensile behaviour of MWCNT reinforced palm oil polyol based shape memory polyurethane



Aula Aqila Yusrizal^a, Tuti Katrina Abdullah^a, Ernie Suzana Ali^b, Sahrin Ahmad^c, Syazana Ahmad Zubir^{a,*}

^a School of Materials and Mineral Resources Engineering, Engineering Campus, Universiti Sains Malaysia, 14300 Nibong Tebal, Penang, Malaysia

^b Department of Physics, Faculty of Science and Technology, Universiti Sains Islam Malaysia, 71800 Nilai, Negeri Sembilan, Malaysia

^c School of Applied Physics, Faculty of Science and Technology, Universiti Kebangsaan Malaysia, 43600 Bangi, Selangor, Malaysia

Received 13 October 2021; accepted 23 March 2022

Available online 31 March 2022

KEYWORDS

Multiwalled carbon nanotubes;
Thermal properties;
Tensile properties;
Polyurethane;
Shape memory polymer

Abstract Shape memory polyurethane (SMPU) has received tremendous interest because of its low cost, low density, as well as easy processing. However, its inferior mechanical properties compared to shape memory alloys have constrained its application in a broad range of engineering areas. Nanofillers are commonly added to polymers to overcome the problem associated with low mechanical characteristics. This study aims to examine the effect of various loadings of multi-walled carbon nanotubes (MWCNT) on the thermal stability, soft segment crystallinity, tensile and shape memory behaviour of palm oil polyol based SMPU nanocomposites. The SMPU nanocomposites were synthesised using a two-step polymerisation process. Microphase-separated SMPU nanocomposites obtained as the differential scanning calorimetric analysis showed two melting transitions, which belonged to the soft and hard phase domains. Furthermore, it was found that MWCNT had acted as a nucleating agent, which promoted the crystallisation process of SMPU nanocomposites. The thermal stability and tensile properties of SMPU/MWCNT nanocomposites were enhanced significantly as the MWCNT was added to the SMPU matrix. A considerable enhancement in the shape fixity (SF) value was revealed for PU-30 and PU-40 samples with the addition of MWCNT. The shape recovery (SR) time of SMPU was faster for samples reinforced with MWCNT, whereas SF increased while SR decreased upon increasing the shape memory cycle.

* Corresponding author at: School of Materials and Mineral Resources Engineering, Engineering Campus, Universiti Sains Malaysia, 14300 Nibong Tebal, Penang, Malaysia.

E-mail address: syazanazubir@usm.my (S. Ahmad Zubir).

Peer review under responsibility of King Saud University.



The SMPU nanocomposites produced demonstrated enhanced thermal and tensile properties, which has the potential as smart material in many industrial applications.

© 2022 The Authors. Published by Elsevier B.V. on behalf of King Saud University. This is an open access article under the CC BY-NC-ND license (<http://creativecommons.org/licenses/by-nc-nd/4.0/>).

1. Introduction

Polyurethanes (PUs) are a versatile class of polymers that can be fabricated into different forms via adjustments of their chemical composition. Hence, they can be utilised in a variety of applications such as textile, automotive, building and construction, electronics, marine, and medical (Rahman et al., 2018; Sánchez-Urbano et al., 2018; Gómez-Rojo et al., 2019; Qiu et al., 2018; Joseph et al., 2018; Oushabi et al., 2017). Most polyurethanes are block copolymers consisting of alternating amorphous or crystalline soft and hard segments due to thermodynamic incompatibility of the two segments. The polyol forms the soft phase, whereas the hard phase develops as a result of the reaction between the chain extender and diisocyanate (Jiang et al., 2018). Since various diisocyanates and polyols are available, manipulating the composition and selection of suitable components allows the creation of a broad spectrum of polyurethanes to be tailored to specific applications (Karak, 2017; Akindoyo et al., 2016). The use of polyols from renewable resources in polymers preparation, such as castor oil, soybean oil, and numerous seed oils, has been widely explored to navigate environmental and safety issues (Malani et al., 2022; Mat Saad et al., 2021; Huang et al., 2021; Zhang et al., 2021). Palm oil polyol has become an important renewable feedstock for low-cost industrial manufacturing of polyols and polyurethane owing to its low price and abundance (Pillai et al., 2016).

The current interest in producing smart polyurethane, particularly with the shape memory effect, enables the material to fix and recover its shape upon exposure to various stimuli. The ability to control its shape places the material at the forefront of multiple research areas extending its applications in biomedical, textiles, aerospace, among others (Trinh et al., 2020; Kumar et al., 2019). Shape memory polyurethane (SMPU), which falls under the category of shape memory polymer (SMP), is known to offer various advantages because it is relatively light in weight, easy to process, non-toxic, biocompatible and has high elastic deformation and recoverable strain than shape memory alloys (Wang et al., 2021a; Hassanzadeh-Aghdam et al., 2019). However, despite the remarkable properties mentioned, they have low mechanical properties, thus limiting their use for industrial applications.

The typical approach to improve the drawbacks mentioned is by incorporating high-modulus nanofillers into the polymer matrix. The influence of nanoparticles in shape memory composites has been reported to affect the nanocomposites' morphology, mechanical properties, and shape memory behaviour (Zhang et al., 2022; Babaie et al., 2019). Carbon nanotube (CNT) has become the highlighted nanoparticle material that can help to improve the existing polymer matrix in achieving excellent shape memory behaviour, thermal and mechanical properties. This is owing to its extraordinary strength, high modulus of elasticity and good thermal behaviour, making it a key material in the nanotechnology field (Díaz et al., 2021).

The addition of nano-scale CNT fillers into a polymer matrix will result in a minute space within the nanofillers compared to a traditional composite filled with micro-sized particles. As such, the properties of the nanocomposite can be effectively modified even at a very low filler content. In most studies on the PU/CNT nanocomposites, the content of the CNT particles ranges between 0.1 and 5 wt%, and the nanocomposite properties obtained has increased by up to 500% compared to the PU without fillers (Yazdi et al., 2019; Chen et al., 2015). Therefore, the CNT content range used in this study is between 0.5 and 2.0 wt%, and the type of CNT was a multi-wall carbon nanotube (MWCNT) with a functional –OH group on its surface to ensure good

dispersion and interactions with the SMPU matrix. Palm oil polyol was incorporated as part of the soft segment and varied between 0 and 40% molar ratio. Its influence on the final properties of SMPU was investigated and reported (Ahmad Zubir et al., 2018).

Considering SMPU's versatility and its numerous industrial applications, as well as safety and environmental concerns regarding the use of petrochemical feedstock in the production of polyurethane, we reported on the synthesis of SMPU with the incorporation of palm oil polyol as part of the soft segment and MWCNT as filler via a bulk polymerisation process. According to our knowledge, there are insufficient studies reported on the effect of MWCNT in palm oil polyol based SMPU nanocomposite so far. Therefore, this work was conducted to further examine the MWCNT particle dispersion in the PU matrix and the effect of its addition on soft segment crystallisation, thermal stability, tensile and the shape memory behaviour of SMPU nanocomposites.

2. Experimental section

2.1. Materials

Polycaprolactone diol (PCL) with molecular weight 4000 g/mol was obtained from Perstorp Polyols (Ohio, United States) under the trade name CAPA 2403D, whereas palm oil polyol (POP) with molecular weight 1000 g/mol was provided by Rovski Sdn. Bhd. (Selangor, Malaysia). Both polyols, PCL and POP, were heated in a vacuum oven at 80 °C overnight before being used to eliminate any moisture present. 4,4'-diphenylmethane diisocyanate (MDI) was supplied by Sigma-Aldrich (Selangor, Malaysia), as well as 1,4-butanediol (BD) and dibutyltin dilaurate (DBTDL). BD was preheated for 2 h at 80 °C prior to use while MDI was used as received. MWCNT with –OH functional group (TNSMH3 grade, 96% purity) was purchased from Chengdu Organic Chemical Co. Ltd. (Chengdu, China). The inner and outer diameters of the MWCNT were 5–10 nm and 10–20 nm, respectively, with a length of 0.5–2.0 µm.

2.2. Synthesis of polyurethane and polyurethane nanocomposites

Polyurethane was synthesised via the two-step prepolymer method (Ahmad Zubir et al., 2018). Firstly, MDI and PCL were mixed at 80 °C in a three-necked flask with an oil bath and mechanical stirrer under nitrogen surrounding. POP (10, 20, 30 and 40% molar ratio) was then added and stirred for 2.5 h at a speed of 100 rpm. In the second step, the prepolymer together with BD and MWCNT (0.5, 1.0, 1.5 and 2.0 wt%) were mixed in an internal mixer at the rotor speed of 90 °C and 50 rpm until the torque plateaued. Finally, the produced polyurethane samples were hot-pressed into a rectangular sheet of 0.5 mm thickness by compression moulding at 160 °C. Pristine SMPU was prepared using the same method but with the addition of DBTDL as a catalyst to replace MWCNT. The monomers and general reaction scheme for the synthesis of SMPU are shown in Fig. 1. The samples were

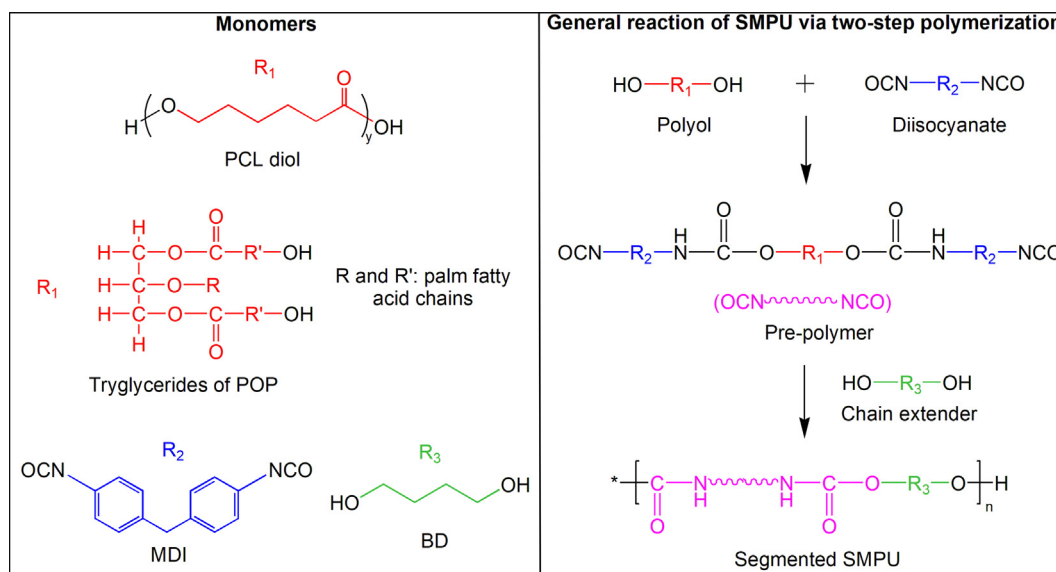


Fig. 1 The monomers and general reaction scheme for the synthesis of SMPU.

coded as PU-X for pristine samples in which X denotes the molar ratio of POP in percentage, whereas, for SMPU nanocomposites, the code used was PU-X-Y in which Y denotes the percentage of MWCNT.

2.3. Characterisations

2.3.1. FTIR analysis

Fourier transform infra-red (FTIR) analysis was performed on the neat SMPU and nanocomposites using Spectrum GX Perkin Elmer. The samples were prepared by dissolving them in DMF solution, and three drops of the solution mixture were placed on the KBr disc. It was then heated in a vacuum oven at 80 °C for 24 hrs. As a result, the FTIR spectrum is recorded between 650 and 4000 cm^{-1} with 4 cm^{-1} resolutions.

2.3.2. Thermal analysis

The thermal behaviour of the pure SMPU and nanocomposites was analysed by differential scanning calorimetry (DSC) and thermogravimetric analysis (TGA). The DSC analysis was measured on Mettler Toledo 822E instrument under two thermal scans. Firstly, the samples were scanned at 20 to 250 °C at a heating rate of 10 °C/min followed by cooling to -100 °C at a cooling rate of 25 °C/min. The second thermal scan was recorded from -100 to 250 °C at 10 °C/min. The TGA thermogram was recorded on the Mettler Toledo-TGA instrument at a temperature range of 20 to 900 °C with 10 °C/min heating rate.

2.3.3. X-ray diffraction analysis

X-ray diffraction (XRD) analysis was conducted on the XRD instrument model Siement D500 with Cu $K\alpha$ ($\lambda = 1.5406 \text{ \AA}$). The samples were scanned at a scattering angle (2θ) from 10 to 35° with a scanning rate of 1°/min and step of 0.025°.

2.3.4. Morphological analysis

The morphological analysis was investigated by transmission electron microscopy (TEM) and field-emission scanning electron microscopy (FESEM). TEM analysis was conducted on the TEM instrument model Hitachi H-7100 at 120 kV. The samples were cut at the cryogenic temperature (-80 °C) into 70 nm thick using a diamond knife. On the other hand, FESEM micrographs of the tensile fracture surfaces were examined on the FESEM instrument model Zeiss/SUPRA 55VP. The cross-section analysis was also performed on a cryogenically fractured surface after immersion in liquid nitrogen for a few minutes.

2.3.5. Tensile testing

The tensile properties of pure SMPU and SMPU nanocomposites were evaluated using the Universal Testing Machine Instron 5567 under the crosshead speed of 50 mm/min on the dumbbell-shaped specimens as per ASTM D 638 (type V).

2.3.6. Shape memory behaviour analysis

The shape memory behaviour of pure SMPU and nanocomposites was investigated using a bending test. A rectangular-shaped sample was heated to 60 °C and bent to form a ring-like structure. It was then immediately immersed into a bath of ice-water at a temperature of about 3 °C while maintaining its shape. The force was removed after 10 min of immersion and the immediate change in the angle of the sample was recorded as force removal angle, θ_{fr} . The sample was finally reheated at 60 °C, and the recovery angle, θ_r , was measured. The shape fixity and shape recovery were calculated based on the θ_{fr} and θ_r using the following equations:

$$\text{Shape fixity (\%)} = \theta_{fr} \div 90^\circ \times 100\% \quad (1)$$

$$\text{Shape recovery (\%)} = (90^\circ - \theta_r) \div 90^\circ \times 100\% \quad (2)$$

3. Results and discussion

3.1. FTIR

FTIR was carried out to investigate the reaction between the PU matrix and MWCNT filler. Fig. 2 shows the FTIR spectrum for MWCNT, PU-20 and PU-20/MWCNT nanocomposite. The FTIR spectrum of MWCNT shows the presence of absorption peaks at wavelengths of 3440 and 1637 cm^{-1} , which refer to the stretching vibration of the -OH group present on the surface of the MWCNT (Senin et al., 2018). -CH_2 stretching peaks were observed between 2980 and 2840 cm^{-1} demonstrating the presence of structural defects in the MWCNT filler, which may have been formed during processing (Chakoli et al., 2009). For PU-20 and PU-20/MWCNT nanocomposites, the peaks are presented in the range of 3320–3340 cm^{-1} and 1700–1725 cm^{-1} due to the presence of NH group and C = O stretching from the ester, respectively (Mahapatra et al., 2013). Peaks at 2941 and 2865 cm^{-1} represent -CH_2 stretching, while other modes of CH vibrations can be found at 1469, 1415, 1365 and 1294 cm^{-1} (Asefnejad et al., 2011). Meanwhile, the peaks at 1596 and 1533 cm^{-1} are represented as the C = C stretching vibrations and the NH bending (amide II), respectively (Javaid et al., 2020). The bands at 1065 and 1046 cm^{-1} are attributed to C-O stretching vibration in urethane (Haryńska et al., 2019) whereas the band at 1172 cm^{-1} is assigned to O-C = O stretching vibration of PCL (El Mahdi et al., 2017).

The absence of NCO peak at a wavelength of 2280 cm^{-1} and the disappearance of OH peak belonging to MWCNT at 3340 cm^{-1} suggest that good interactions have taken place during the production of SMPU/MWCNT nanocomposite. Moreover, the observed NH peaks at 3320 and 1530 cm^{-1} also indicates the presence of a urethane network in SMPU/MWCNT nanocomposite. The positions of the peaks for PU-20 and PU-20 nanocomposite samples remained unchanged, while the peak intensity was found to have increased with increases in the MWCNT content. This may be closely related to the physical interactions as the hydrogen bonds are formed between the -OH group of MWCNT with the C-O of PU matrix (Fig. 3) (Hajjalizadeh et al., 2017). Tijjing et al. (2013) also obtained similar findings in the study of PU/MWCNT nanocomposite prepared by electrospinning and solution casting. In addition, as the content of MWCNT

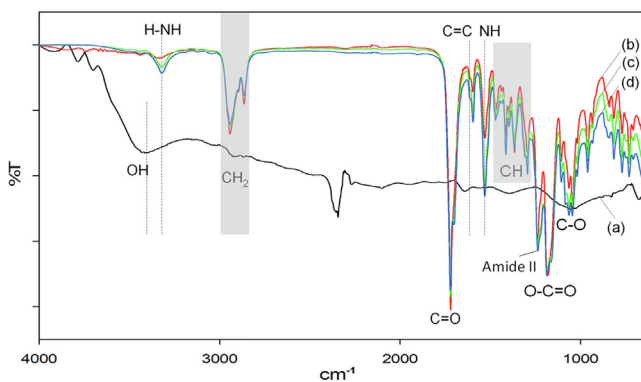


Fig. 2 FTIR spectra for (a) MWCNT, (b) PU-20, (c) PU-20/1.0% MWCNT, and (d) PU-20/2.0% MWCNT.

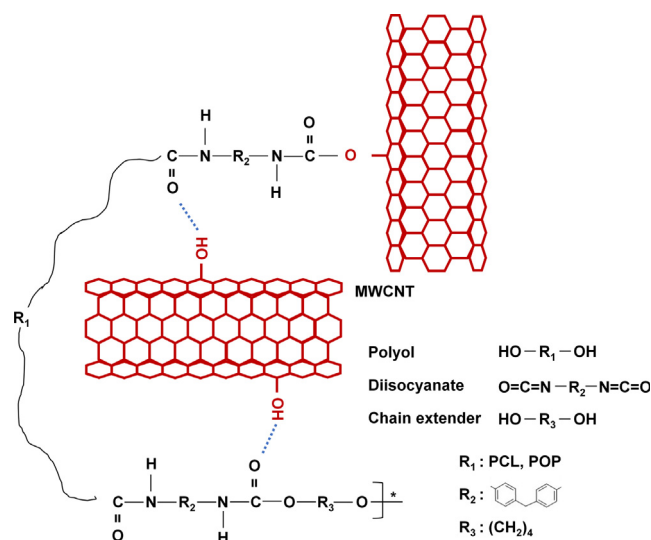


Fig. 3 Possible interactions between MWCNT and SMPU.

is increased, a significant increase in intensity was observed for the amide II peak at 1533 cm^{-1} . This may be due to the increased formation of urethane networks as a result of interactions between the -OH group on the surface of the MWCNT and isocyanates (Fig. 3).

The analysis of the hydrogen bonding was carried out by using FITYK software to calculate the ratio of the area under the peak for the carbonyl group. $A_{\text{HCO}}/A_{\text{CO}}$, which is the ratio of the area of the hydrogen-bonded carbonyl (HCO) group to the total area of the carbonyl group (HCO + FCO), was calculated and tabulated in Table 1. The stretching absorption of the H-CO group appeared at 1703 cm^{-1} , while the FCO stretching was around 1723 cm^{-1} .

For all SMPU samples, the H-CO peaks increase with the addition of more MWCNT content, while the FCO peaks decrease. Therefore, the $A_{\text{HCO}}/A_{\text{CO}}$ values in Table 1 are found to have increased with increasing filler content. The increase in the $A_{\text{HCO}}/A_{\text{CO}}$ values indicates that there had been an increment in the hydrogen bonding interactions between the MWCNT and the PU matrix with an addition of more MWCNT content. Furthermore, with the increase of the POP content, the $A_{\text{HCO}}/A_{\text{CO}}$ values also increase, implying that more hydrogen bonds have been formed between the carbonyl of POP and NH of urethanes with the increase of POP content.

3.2. Thermal properties

Thermal properties, such as melting point and heat of fusion, were obtained through the use of DSC, while thermal stability properties were analysed using a TGA thermogram. The DSC analysis for the SMPU and SMPU/MWCNT nanocomposite involved a heating-cooling-heating process. Thus, two heating scans were recorded during the DSC analysis. Table 2 shows the data for the melting point, T_m , and the heat of fusion, ΔH_m , obtained during the analysis. Two endothermic peaks were obtained in this test. The first peak at a temperature of $\sim 45^\circ\text{C}$ and the second peak at $\sim 160^\circ\text{C}$ represent the melting point of the crystalline soft segment and hard segment, respectively (Asensio et al., 2019; Wang et al., 2021b).

Table 1 A_{HCO}/A_{CO} for SMPU and SMPU/MWCNT nanocomposites.

MWCNT (%)	PU-0	PU-10	PU-20	PU-30	PU-40
0	0.36	0.38	0.40	0.40	0.44
0.5	0.37	0.40	0.41	0.42	0.45
1.0	0.37	0.41	0.41	0.45	0.45
1.5	0.38	0.41	0.42	0.46	0.46
2.0	0.38	0.42	0.43	0.46	0.47

For the melting of the PCL crystalline soft segment, the T_m values for scan 2 (temperature range 36–46 °C) show lower values compared to scan 1 (temperature range 45–51 °C) due to the rapid cooling effect. The T_m values for scan 2 show a considerably clearer pattern. Samples containing POP gave lower T_m values compared to the SMPU without POP (PU-0), and this pattern continues with the addition of more POP content. This may be due to the presence of POP content that contributes to the formation of hard segments, preventing the formation and growth of PCL crystals. Meanwhile, for all the SMPU samples, the ΔH_m value is found to increase with the increasing MWCNT. This indicates that the MWCNT acts as a nucleation site that promotes the crystallisation of the PCL soft segment (Richardson et al., 2011; Trujillo et al., 2012).

For all the SMPU samples, increasing the MWCNT content increases the T_m of the hard segments (Table 2). The T_m of the hard segment increases to ~ 30 °C with the addition of the MWCNT compared to the SMPU without any filler. This

implies that the filler tends to react with the hard segments that are more polar, and it assists in the crystallisation process (Richardson et al., 2011; Sahebi Jouibari et al., 2018). Moreover, Tijing et al. (2013) also reported that the interaction between the hard segments and the MWCNT through these newly-formed hydrogen bonds stabilised the dynamic nanocomposites' thermal properties, causing the T_m values to increase following the increase in the amount of MWCNT. The ΔH_m of the hard segment increased with the addition of more MWCNT content, which suggests that more short-ranged hard segments were formed by the addition of MWCNT, where its presence served as a nucleating agent for the crystallisation of the hard segments.

The thermal stability analysis of SMPU/MWCNT nanocomposite is shown in Fig. 4 and Table 3 for the PU-0 and PU-20 samples. In addition, a TGA analysis was carried out on the MWCNT sample, and the results show that the MWCNT experiences a loss in weight of up to 20% at temperatures of between 70 and 600 °C (Fig. 5). This weight loss is closely associated with the thermal degradation of the OH group present on the surface of the MWCNT.

Based on the differential thermogravimetric (DTG) analysis in Fig. 4, three significant peaks are noticed for SMPU/MWCNT nanocomposite compared to the SMPU without filler, with only two peaks. In reference to this, it can be concluded that the SMPU/MWCNT nanocomposite experienced three stages of degradation during the decomposition process, while the SMPU without filler experienced two stages of degradation. The first stage of degradation for the SMPU/MWCNT nanocomposite occurs at the temperature

Table 2 Thermal properties of SMPU and SMPU/MWCNT nanocomposites.

Sample	Soft segment				Hard segment	
	Scan 1		Scan 2		Scan 1	
	T_m (°C)	ΔH_m (J/g)	T_m (°C)	ΔH_m (J/g)	T_m (°C)	ΔH_m (J/g)
PU-0	49	31.3	46	29.6	154	3.0
PU-0-0.5	51	35.8	45	31.7	193	8.3
PU-0-1.0	50	32.8	45	31.2	189	5.6
PU-0-1.5	52	37.4	46	30.7	191	7.4
PU-0-2.0	51	33.1	46	29.2	191	6.3
PU-10	47	30.5	45	27.7	160	3.4
PU-10-0.5	46	35.9	45	32.3	187	9.0
PU-10-1.0	53	36.1	46	30.7	190	8.4
PU-10-1.5	46	35.4	45	30.8	190	8.6
PU-10-2.0	51	37.7	46	30.2	189	7.6
PU-20	47	28.3	45	26.7	184	4.5
PU-20-0.5	50	32.9	44	28.5	192	6.5
PU-20-1.0	49	31.4	43	27.8	191	7.7
PU-20-1.5	51	30.9	43	27.4	190	6.8
PU-20-2.0	50	32.1	45	26.9	189	7.5
PU-30	46	23.2	43	21.5	158	4.9
PU-30-0.5	49	28.3	43	25.6	188	8.8
PU-30-1.0	45	24.2	43	24.4	191	8.9
PU-30-1.5	44	27.9	43	24.3	188	8.7
PU-30-2.0	49	29.4	43	23.3	188	8.1
PU-40	46	20.2	42	17.2	163	5.8
PU-40-0.5	49	26.7	42	21.6	186	9.9
PU-40-1.0	–	–	42	19.3	189	9.0
PU-40-1.5	–	–	42	20.0	187	9.4
PU-40-2.0	–	–	42	12.4	186	7.9

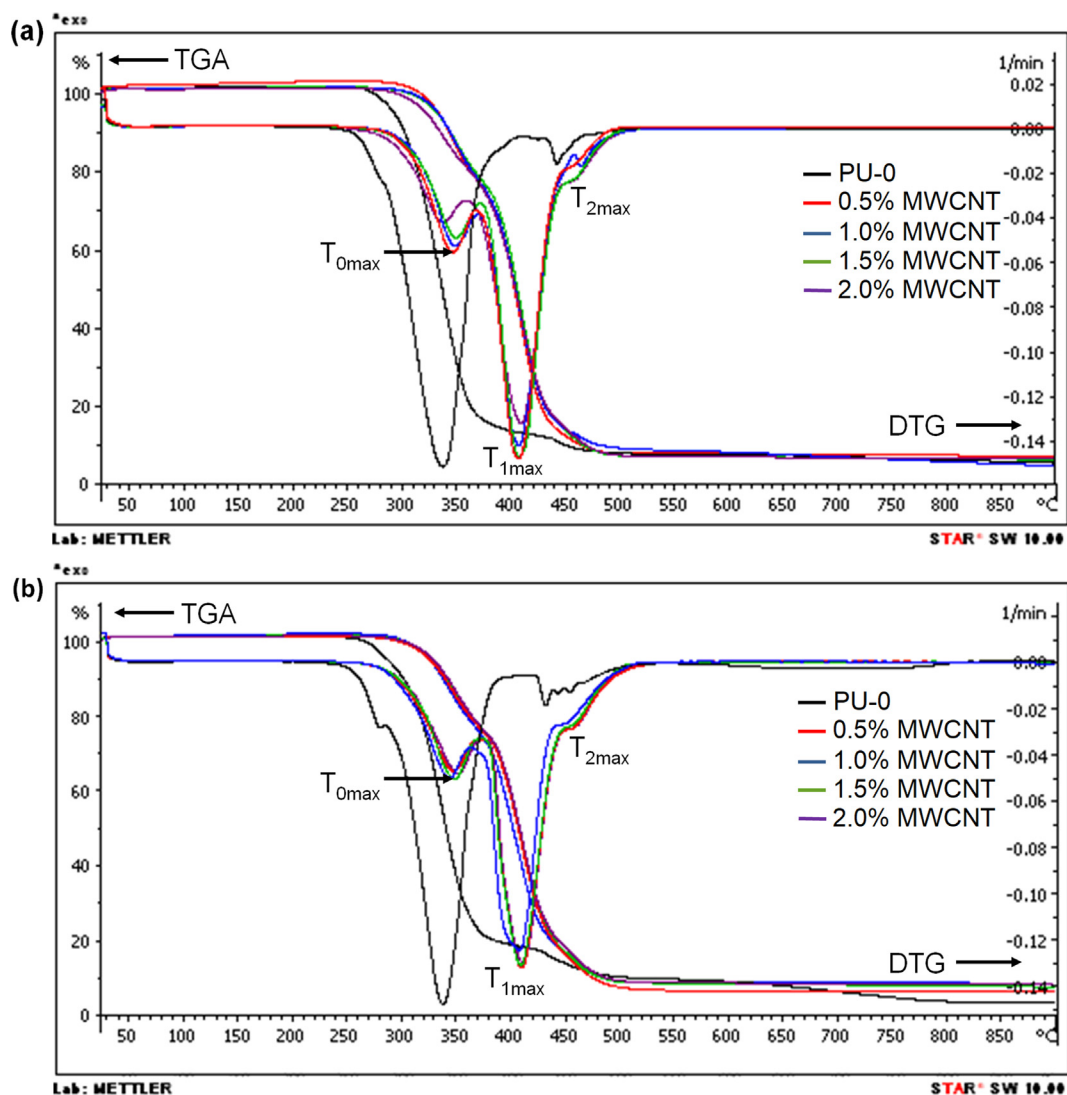


Fig. 4 TGA and DTG thermograms for (a) PU-0 and (b) PU-20 nanocomposites with MWCNT filler.

T_{0max} , which is absent for the SMPU without filler. This stage involves the decomposition of the $-OH$ group present on the surface of the MWCNT. Meanwhile, the second stage of degradation occurs at the temperature T_{1max} , which is the temperature at the maximum degradation rate. At this stage, the main degradation occurs, which involves the decomposition of the urethane network into isocyanate and polyol components (Błażek et al., 2020). The T_{1max} peak of SMPU/MWCNT nanocomposite increases by as much as ~ 60 °C compared to the SMPU without filler (shown by the arrow in Fig. 4), thus indicating that the SMPU nanocomposite's thermal stabilisation improved by the presence of filler. The third stage, which occurred at T_{2max} temperature, involves the breakdown of the ester and aromatic groups inside the PU matrix (Abolins et al., 2018).

The values of T_{0max} , T_{1max} and T_{2max} for all the SMPU samples clearly increased with the addition of filler content by as much as 0.5 wt%, but further increases in the filler content did not have a significant impact on these values. Nevertheless, the residue percentage increased with an increase in the filler content. The residue percentage at 900 °C of the PU-20 sample increased from 3.5% for pure PU-20 to 6%

and 8% with the inclusion of 0.5 and 1.0 wt% filler, respectively. The presence of MWCNT as a thermal insulator, which was uniformly dispersed in the PU matrix, has delayed the thermal degradation (Kumar and Jindal, 2019). This is because of the strong PU/MWCNT interface interaction inhibited the movement of the polymer chain segments, thus forcing the volatile degraded substances to move farther in a zigzag route to bypass the matrix (Jeong et al., 2008).

Moreover, based on Table 3, the temperature at 80% weight loss, $T_{80\%}$, for all the SMPU samples was found to increase with the addition of the MWCNT content. Jin et al. (2007) stated that the MWCNT that interacted with the PU matrix acted as a physical cross-link point which restrained the movement of the polymer chains. This, in turn, caused an enhancement of the thermal stability of the polymer nanocomposites.

3.3. Soft segment crystallisation

One important aspect of this study was the analysis of the PCL soft segment crystallisation as it is closely related to shape memory properties, which is the main focus of the study.

Temp. (°C)	PU-0	PU-0-0.5	PU-0-1.0	PU-0-1.5	PU-0-2.0
T _{0max}	–	350	352	353	340
T _{1max}	340	410	410	411	411
T _{2max}	446	455	467	456	458
T _{80%}	365	430	433	436	438
	PU-10	PU-10-0.5	PU-10-1.0	PU-10-1.5	PU-10-2.0
T _{0max}	–	354	348	351	352
T _{1max}	350	411	411	411	411
T _{2max}	433	455	462	453	454
T _{80%}	391	440	433	435	441
	PU-20	PU-20-0.5	PU-20-1.0	PU-20-1.5	PU-20-2.0
T _{0max}	–	349	346	351	353
T _{1max}	340	411	407	411	412
T _{2max}	436	456	449	454	456
T _{80%}	395	440	441	443	449
	PU-30	PU-30-0.5	PU-30-1.0	PU-30-1.5	PU-30-2.0
T _{0max}	–	349	350	346	349
T _{1max}	342	411	409	409	410
T _{2max}	448	457	450	451	456
T _{80%}	406	448	451	449	452
	PU-40	PU-40-0.5	PU-40-1.0	PU-40-1.5	PU-40-2.0
T _{0max}	–	347	346	341	343
T _{1max}	348	409	409	409	407
T _{2max}	433	453	451	451	451
T _{80%}	422	450	450	458	458

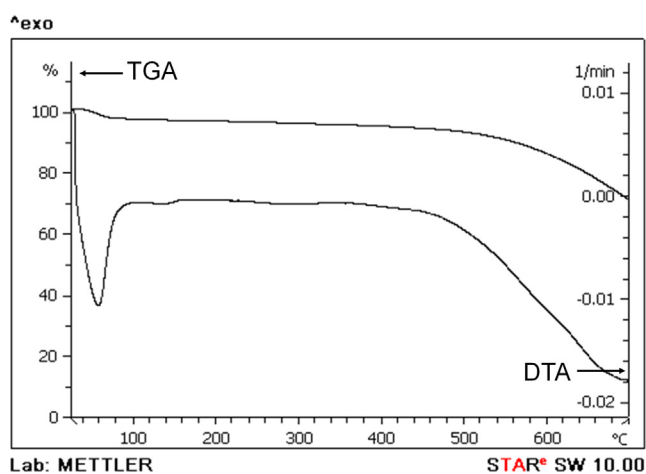


Fig. 5 TGA and DTG thermograms for MWCNT.

PCL segment is responsible for forming crystal structure to set temporary shape at low temperatures, thus allowing the melting point of the PCL segment to be used to control the shape recovery temperature (Shirole et al., 2018). In addition, the crystallisation of the polymer soft segment influences the material's mechanical properties, notably the modulus and hardness. Therefore, the analysis of the soft segment crystallisation was performed based on the DSC and XRD results obtained.

The heat of fusion of PCL obtained from the DSC results are related to the percentage of soft segment crystallinity in

the polymer by taking into account the amount of heat of fusion for 100% crystalline PCL. In other words, the higher the heat of fusion obtained, the more crystal structures are formed in the polymer system (Yadav et al., 2012). Fig. 5 shows the percentage of PCL soft segment crystallinity based on the heat of fusion obtained from scan 2 in Table 2. As expected, the percentage of crystallinity was decreased with increasing POP content since the PCL content, which contributed to the soft segment crystallinity of SMPU, was reduced with the increase of POP content.

The percentage of crystallinity for all the SMPU samples was noticed to rise with an increment in the MWCNT content in the polyurethane system. The PU-10 sample had 20.4% soft segment crystallinity and this rose to 23.8% and 22.6% with the addition of 0.5 and 1.0 wt% MWCNT content, respectively. This is due to the fact that the MWCNT acts as a nucleation site that promotes the PCL soft segment crystallisation process (Cai et al., 2013; Mahapatra et al., 2013; Mondal and Hu, 2006; Rana et al., 2008). These results indicate that the nucleation effect induced by the MWCNT in the PU matrix is due to the formation of strong bonding between filler and PU matrix through hydrogen bonding (Yadav et al., 2012).

Meanwhile, at high filler content, the MWCNT, acting as a physical constraint on the PU molecule, prevented the movement of soft segments during crystallisation (Meng et al., 2009). This was due to the van der Waals attraction among the MWCNT promoting coagulation at higher filler content. Although this coagulation disturbed the soft segment crystallisation, some of the MWCNT was still well dispersed to allow PCL crystallisation to occur. Therefore, the crystallinity percentage decreased slightly at higher filler content.

An XRD analysis was performed to support the results obtained in the DSC analysis. Fig. 7 shows an XRD diffractogram of the MWCNT, PU-0 sample and PU-0/MWCNT nanocomposite. Ghahremani et al. reported that two diffraction peaks were indicated by MWCNT, at position 2θ of 25.8° and 42.9° with reference to the (002) and (100) planes, respectively belonging to the carbon atom that marks the distance between layer 0.34 and 0.21 nm (Ghahremani et al., 2022). Meanwhile, the peaks for the PU-0 and PU-0 nanocomposite that existed at 2θ of 21.3° and 23.6° refer to the (110) and (200) planes of PCL crystals, respectively (Castilla-Cortázar et al., 2019). The addition of MWCNT increased the intensity of the (110) and (200) peaks, with no change in their positions. Similar findings were obtained for all other SMPU nanocomposite samples, and these are displayed in the Supplementary file. This indicates that the crystallisation of PCL increased with an increase in MWCNT. It also indicates that a better arrangement of the polymer chains can be achieved if the MWCNT is dispersed evenly in the PU matrix. Moreover, there was no visible MWCNT peak in the SMPU/MWCNT nanocomposite diffraction. This may be closely related to the use of a very low MWCNT content of only 2.0 wt% (Su et al., 2021).

3.4. Tensile properties

The mechanical properties of a nanocomposite are influenced by a few aspects, for instance, the dispersion and position of the filler, filler aspect ratio, domain size, and the nature and degree of compatibility (Sahoo et al., 2007). Fig. 8 and Fig. 9 show the breaking strength and strain at break of the SMPU/MWCNT nanocomposite. The addition of MWCNT, even at a low content (0.5 wt%), has managed to increase the tensile properties of the nanocomposite to the maximum value. The unique characteristics of MWCNT - high aspect ratio, large surface area, high strength and surface functionality contributed to the enhancement of tensile properties of the nanocomposites. The high aspect ratio of MWCNT provided large surface area for the interactions with SMPU matrix, while the presence of surface functionality on MWCNT

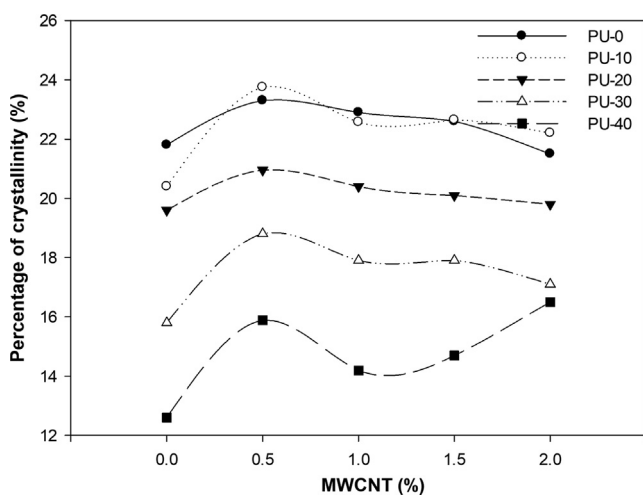


Fig. 6 Percentage of PCL soft segment crystallinity for SMPU/MWCNT nanocomposite.

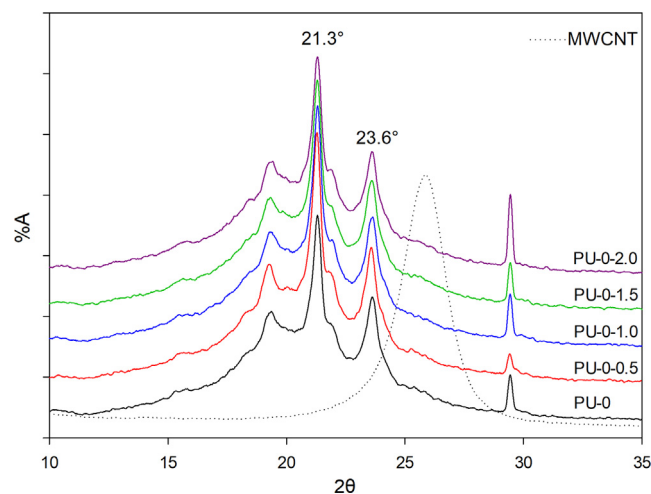


Fig. 7 XRD diffractogram for MWCNT, PU-0 and PU-0/MWCNT nanocomposite.

permitted good dispersion of MWCNT in SMPU matrix since MWCNT able to interact with polymer matrix. The presence of surface functionality on MWCNT and large surface area allowed the formation of great interface adhesion between the matrix and the nanofiller, thereby increasing the efficiency of the load transfer from SMPU matrix to the nanofiller. The addition of high strength MWCNT contributed to strong nanocomposites due to the nano-reinforcement effect of MWCNT.

Fig. 8 displays the breaking strength of SMPU and the SMPU/MWCNT nanocomposites. The breaking strength for all the SMPU samples increased at 0.5 wt% MWCNT content and dropped with a further increase in filler content. PU-0 and PU-20 showed an increase of 24% and 16%, respectively, at 0.5 wt% MWCNT. The increased breaking strength of a nanocomposite is closely related to its capability to convey the tensile load from PU matrix to the filler. This occurs due to the increased interfacial interactions between the MWCNT surface and the PU chain as a uniform filler distribution was

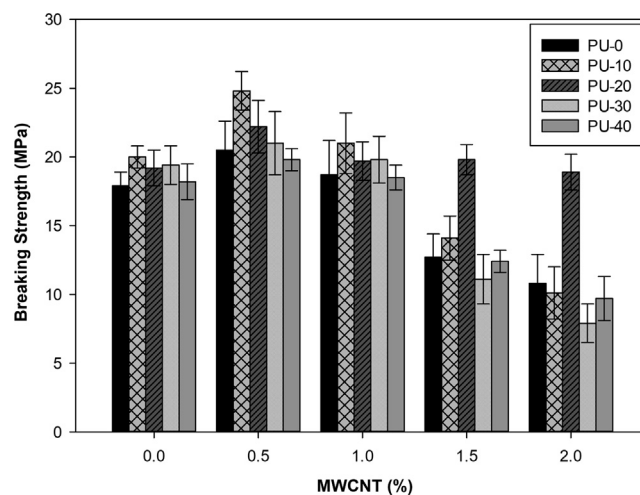


Fig. 8 Breaking strength of SMPU and SMPU/MWCNT nanocomposite.

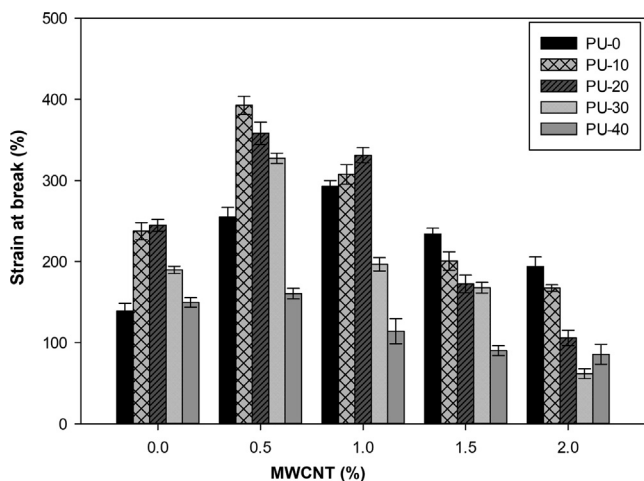


Fig. 9 Strain at break of SMPU and SMPU/MWCNT nanocomposite.

achieved in SMPU with 0.5 wt% MWCNT (Fig. 10 (a,c)). In addition, the orientation and aspect ratio of MWCNT also influence the effective load transfer in the MWCNT-filled PU nanocomposites (Tijing et al., 2013).

Two factors may influence the increase in the breaking strength of the SMPU/MWCNT nanocomposite as mentioned by Tijing et al. (2013). First, structural defects appear on the surface of the MWCNT after the acid treatment process. These structural defects act as an interlocking site between the surfaces of the MWCNT and the PU matrix. Second, the acid treatment attaches the $-\text{COOH}$ functional group to the surface of the MWCNT- COOH , which may lead to an increase reaction between the MWCNT and the PU chains. The presence of structural defects and moiety on the MWCNT increases the number of sites of interaction along the nanofillers with the PU matrix, thereby increasing the load transfer efficiency from PU to the MWCNT (Su et al., 2021).

Meanwhile, in this study, the MWCNT that was used had an $-\text{OH}$ group on its surface. The $-\text{OH}$ group in the MWCNT was likely to interact either covalently or physically with the SMPU chain as shown in Fig. 3. The covalent bond interaction between the $-\text{OH}$ group in the MWCNT with isocyanate would produce a urethane network while the hydrogen bonds formed between $-\text{OH}$ on the MWCNT surface and $\text{NH}/\text{C}=\text{O}$ belonging to urethane would form physical cross-links. Based on the technical data obtained from the supplier, the MWCNT-OH that was used had been prepared by the oxidation of KMnO_4 in a solution of H_2SO_4 . The oxidation of CNT in a mixture of $\text{KMnO}_4/\text{H}_2\text{SO}_4$ will provide defect sites, and the opening of nanotube ends (Yang et al., 2018; Poudel and Li, 2018). This suggests that structural defects are formed on the MWCNT walls, which can promote the formation of interlocks between the SMPU chain and the MWCNT. The presence of structural defects in the MWCNT has been shown by FTIR analysis, which has been discussed previously. Therefore, the increase in breaking strength is achieved.

Tijing et al. (2013) also reported that straight-shaped MWCNT uniformly dispersed in the polymer matrix is more capable of transferring loads than curled and agglomerated MWCNT. This study observed MWCNT clumps in the PU-20

samples with 2.0 wt% MWCNT content through morphological analysis, as shown in Fig. 10 (b, d). This phenomenon explains the decrease in breaking strength obtained at high filler content (1.5–2.0 wt%) due to the inability to transfer the load effectively. In fact, the breaking strength obtained was lower than that obtained by the SMPU without filler.

The clump formation tendency of MWCNT at high filler content is owing to the existence of the van der Waals attraction among the MWCNT particles. These clumps can begin to cause cracks, which then propagate easily. The presence of these cracks will usually lower the strength of the nanocomposite as a whole. However, the breaking strength of the PU-20 nanocomposite on the filler content of 1.5–2.0 wt% showed a very high value when compared with the other PU samples. This suggests that a very good MWCNT/PU matrix interface interaction was achieved in the SMPU through the formation of interlocks between the SMPU chain and the MWCNT compared to other samples at the same filler content.

Fig. 9 shows the strain at break values obtained for the SMPU and the SMPU/MWCNT nanocomposite. The strain at break for PU-0 increased with the addition of filler content, while the other SMPU samples showed a maximum value at 0.5 wt% filler content. The PU-0 and PU-10 showed an increase of 111% and 66% with the addition of 1.0 and 0.5 wt% MWCNT, respectively, compared to the SMPU without filler. The attainment of a high strain at break in the SMPU sample containing POP compared to pure SMPU was due to the presence of slightly branched structures belonging to the POP between the PU chains which enhanced the mobility of the polymer backbone chains. In addition, the spacing between the polymer chains facilitated the disentanglement of the chains during sample deformation.

The good increase in strain at break is said to be closely linked to the existence of an excellent interface reaction between the polymer matrix and filler, so strong such that the filler acts as an extended chain to the PU molecules, therefore increases the entanglements density that are trapped in the physical network (Richardson et al., 2011). In this study, the $-\text{OH}$ moiety on the surface of MWCNT is compatible to react with the polar PU matrix, hence expected to form strong bond during processing.

However, with further addition of filler content, even in the presence of a slightly branched POP structure, the MWCNT is more likely to form clumps that will reduce the interface interaction of the filler/PU and thus reduce the effective load transfer. Furthermore, at high MWCNT content (1.5–2.0 wt%), the strain at break of the SMPU nanocomposite was lower than that of the SMPU without filler. This strain at break had the same trend as the breaking strength. In this case, the MWCNT present was no longer acted as a reinforcing agent, but instead it became a contributing factor to the failure of the SMPU nanocomposite due to agglomeration. Thus, the reduction in the strain at break with a further increase in the amount of MWCNT at higher loading may also have been caused by increased restrictions on the movement of molecules in the polymer chains with the presence of MWCNT (Deka et al., 2010). The PU-30 sample showed a significant decrease in the strain at break at 2.0 wt% of MWCNT content compared to other samples. This suggests that at 2.0 wt% MWCNT content, the PU-30 achieved high rigidity compared to other samples due to the presence of MWCNT clumps.

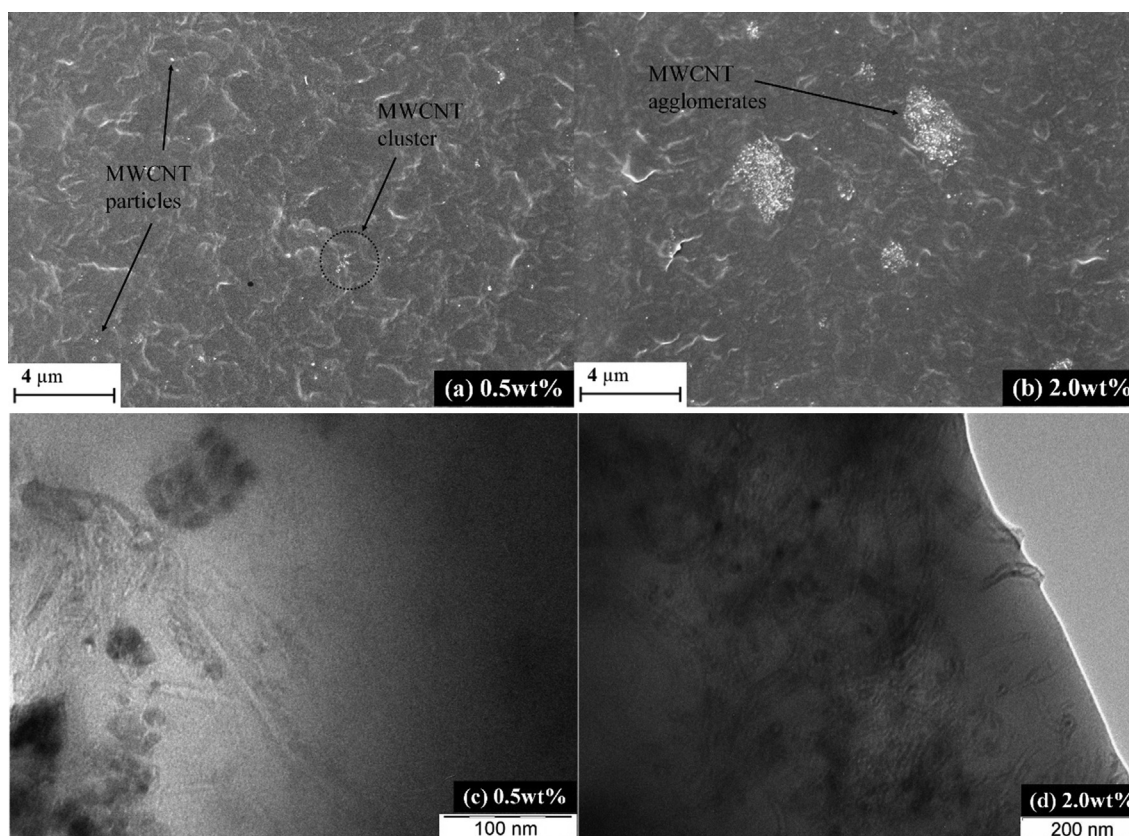


Fig. 10 (a, b) TEM micrographs and (c, d) FESEM micrographs of PU-20 nanocomposite with 0.5 wt% MWCNT and 2.0 wt% MWCNT.

A morphological analysis was also conducted on a tensile fracture specimen and cryogenically fractured sample to obtain information on the relationship between the structure and the characteristics of the resultant SMPU (Fig. 11 and Fig. 12). The surface of the stretched sample shows the presence of bright spots and lines that refer to the MWCNT particles (Fig. 11). Furthermore, the structure of the MWCNT with broken ends was obtained in the SMPU sample with 0.5 wt% filler content, while the pulled-out structure was found in the SMPU with 2.0 wt% MWCNT filler. This observation suggests that the interaction between the MWNT and the PU matrix was very strong in the SMPU nanocomposite with 0.5 wt% filler content compared to 2.0 wt% MWCNT (Su et al., 2021).

Based on FESEM micrographs of the cryogenically fractured surface of PU-20 nanocomposite in Fig. 12, the nanocomposite with 2.0 wt% MWCNT filler showed rougher surface than the 0.5 wt% filled nanocomposites. This was closely related to the formation of a new surface area due to the switching of the crack trajectory caused when the amount of rigid fillers is increased (Richardson et al., 2011). The same thing was also observed in the FESEM micrograph of the tensile fractured surface in Fig. 11.

3.5. Shape memory properties

An analysis of shape memory properties was conducted to determine the influence of MWCNT addition on the behaviour

of the shape memory of SMPU nanocomposites. In SMPU, the hydrogen-bonded hard segment phase is accountable for shape recovery, whereas the soft segment phase is crucial for shape fixity (Yap et al., 2021). For SMP, to acquire the shape memory properties, the polymer should have the optimum degree of chemical cross-links to form a memory network or contain a sufficient fraction of crystals that act as physical cross-links (Reghunadhan et al., 2021). In this study, the interactions between the urethane hard segments formed physical cross-links that were in charge of preserving the original form of the SMPU, while the crystallisation of the PCL soft segment fixed the temporary shape when the sample was cooled to a temperature $< T_m$ PCL.

Based on the literature, the shape fixity properties of a T_m -SMP depends on two factors; the degree of soft segment crystallinity and the modulus at room temperature (Gunes et al., 2008). Tables 4 and 5 illustrate the shape memory behaviour for SMPU and the SMPU/MWCNT nanocomposite. Based on Table 4, the shape fixity properties for PU-0, PU-10 and PU-20 with their nanocomposites achieved 100%. This shows that the total percentage crystallinity in this SMPU system (between 19 and 24%) was sufficient to fix the temporary form and was also enough to overcome the retraction angle induced by the presence of 'unlocked' chains that result in immediate withdrawal when the load is removed. Therefore, no angle of retraction is observed for the PU-0, PU-10 and PU-20 samples.

Meanwhile, the PU-30, PU-40 samples and their nanocomposites with a percentage of crystallinity below 19% failed to

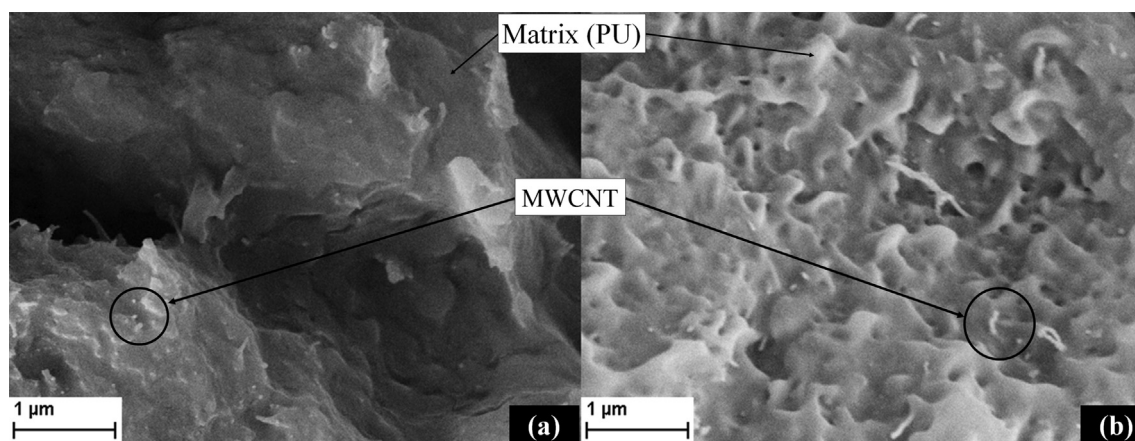


Fig. 11 FESEM micrograph of tensile fractured PU-20 nanocomposite sample with (a) 0.5 and (b) 2.0 wt% MWCNT filler.

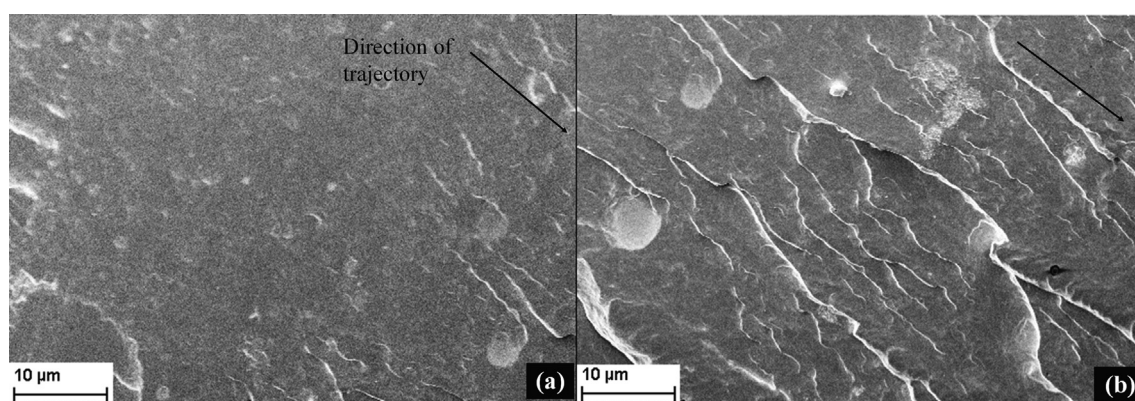


Fig. 12 FESEM micrograph of cryogenically fractured PU-20 nanocomposite sample with (a) 0.5 and (b) 2.0 wt% MWCNT filler.

show 100% shape fixity. Nevertheless, the shape fixity increases with the addition of MWCNT particles, with a consistent increase in the percentage of crystallinity, as shown in Fig. 6. The shape fixity of PU-30 and PU-40 rose to 99.6% and 92.2%, respectively, with the addition of 0.5 wt% of MWCNT, with the shape fixity value for the PU nanocomposite being higher than that of the SMPU without filler for both samples. This shows that the interaction between the MWCNT and the PCL soft segments promoted the crystallisation of PCL. A small number of MWCNT particles acted as a nucleus for the heterogeneous nucleation of crystallisation, thus enhancing the crystallisation process (Trujillo et al., 2012). Garle et al. (2012), in their study, concurred that soft segment

crystallisation is one of the significant factors for the SMP to display shape memory behaviour.

Table 5 shows the shape recovery properties for all SMPU and SMPU/MWCNT nanocomposites. All the SMPU samples demonstrated excellent shape recovery of up to 100%. Fig. 13 demonstrates the finding in Table 4-5 for the PU-40 samples. Good shape recovery is achieved despite the existence of MWCNT clumps with the high filler content. This is due to the existence of structural defects and -OH moiety on the surface of the MWCNT that interact strongly with the PU matrix. Therefore, no deterioration in the shape recovery was observed for the SMPU/MWCNT nanocomposite.

3.6. Shape recovery time and shape memory cycle.

The analysis of shape recovery time and shape memory cycle was performed on all pristine SMPU and PU-30 nanocomposites since the shape fixity value of PU-30 did not show 100%. The time taken by an SMP material to return to its original shape after reheating is known as the shape recovery time. In this test, two heating methods were used to heat a ring-shaped temporary sample. In the first method, the sample was placed in hot water with a temperature of 50 °C and the second method, the sample was placed on the surface of a hot-plate that has been heated to a temperature of 50 °C. The time taken for the samples to recover to their original form was

Table 4 Shape fixity of the SMPU/MWCNT nanocomposites.

MWCNT (wt%)	PU-0	PU-10	PU-20	PU-30	PU-40
0	100	100	100	94.4	84.4
0.5	100	100	100	99.6	92.2
1.0	100	100	100	99.3	90.0
1.5	100	100	100	99.3	85.0
2.0	100	100	100	97.8	87.3

Table 5 Shape recovery of the SMPU/MWCNT nanocomposites.

MWCNT (wt%)	PU-0	PU-10	PU-20	PU-30	PU-40
0	100	100	100	100	100
0.5	100	100	100	100	100
1.0	100	100	100	100	100
1.5	100	100	100	100	100
2.0	100	100	100	100	100

recorded using a video camera and displayed in [Table 6](#) and [Fig. 14](#).

Based on [Table 6](#), the shape recovery time for samples immersed in hot water is found to be shorter than samples placed on the surface of the hotplate. The shape recovery time for the SMPU samples immersed in hot water is between 2 and 6 s compared to the 33–50 s time required for samples placed on the surface of the hotplate to return to their original shape. For the SMPU samples immersed in hot water, the entire surface of the sample was in contact with the hot water, resulting in a more effective heat transfer. Therefore, a short time was required to return to its original shape. [Fig. 14a](#) shows the deformation experienced by PU-30 and 1.0% MWCNT filled PU-30 nanocomposites while immersed in hot water at a temperature of 50 °C. Meanwhile, for the SMPU samples placed on the surface of the hotplate, only a small portion of the sample surface is in contact with the surface of the hotplate as shown in [Fig. 14b](#). Thus, a longer time is required for the heat to move throughout the sample and melt the soft segment PCL crystals and restore the original shape of the SMPU.

The trend of the shape recovery time of SMPU with the addition of POP content and MWCNT particles is the same for both heating methods. For the SMPU samples, adding POP content up to 20% molar ratio (PU-20) increases the time taken to return them to their original shape, while further addition of POP content subsequently lowers the shape recovery time. On the other hand, the shape recovery time of SMPU nanocomposites decreases with the addition of MWCNT content. The addition of 0.5 and 1.5 wt% of MWCNT reduces the shape recovery time by 2 and 6 s compared to the SMPU without filler in the second heating method. This is closely related to the high thermal conductivity of MWCNT ([Cai et al., 2013](#)). Therefore, the MWCNT -filled SMPU can absorb heat better and faster, thereby speeding up the shape recovery process. Furthermore, good interface interactions between the MWCNT and the PU matrix allows effective heat transfer. At the same time, for example, 20 s (referring to the second

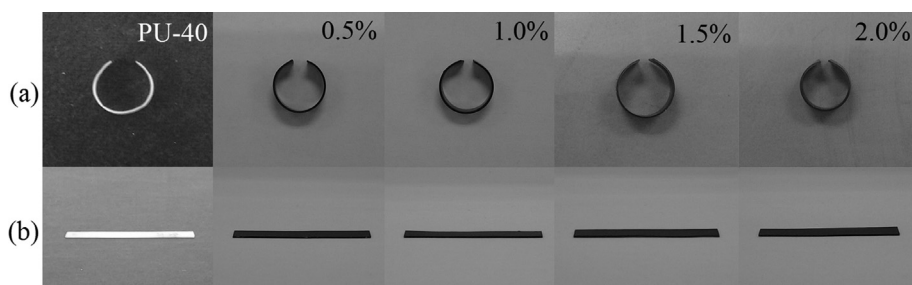
Table 6 Shape recovery time of PU-30 and its nanocomposites.

Sample	Shape recovery time (s)	
	50 °C water	Hotplate surface
PU-0	2.33 ± 0.47	43.67 ± 1.70
PU-10	3.00 ± 0.82	48.00 ± 0.82
PU-20	5.33 ± 0.47	49.67 ± 1.70
PU-30	3.67 ± 0.47	44.33 ± 1.25
PU-40	2.67 ± 0.47	40.00 ± 0.82
PU-30		
0.5% MWCNT	3.33 ± 0.47	42.00 ± 0.82
1.0% MWCNT	3.00 ± 0.82	38.00 ± 0.82
1.5% MWCNT	2.67 ± 0.47	36.00 ± 0.82
2.0% MWCNT	2.00 ± 0.82	33.00 ± 0.82

heating method), the angular openings of MWCNT -filled SMPUs are larger than those SMPU without filler ([Fig. 14b](#)).

Shape memory cycle test was conducted to analyse the degradation of SMPU shape memory performance by repeating the shape memory testing for 3 cycles ([Table 7](#)). For all SMPU samples, it is found that the shape fixity (SF) increases while the shape recovery (SR) decreases with the increase in the number of cycles. For example, PU-30 has 94.4% shape fixity in Cycle 1, which increases to 96.7% and 100% in Cycle 2 and 3. This increase is closely related to the increase in the total crystallinity of the PCL soft segment ([Fig. 15](#)). When a bending load is applied at a high temperature, the bending strain will increase the orientation of the polymer chain ([Kim et al., 1996](#)). This promotes the crystallisation process during cooling, and hence a higher shape fixity is obtained with an increasing number of cycles.

All the SMPU samples with POP addition have initially shown 100% shape recovery experience a significant reduction in Cycle 2 and in subsequent cycles. The shape recovery of PU-0 decreased by 5% and 8.3% in Cycle 2 and Cycle 4. In this study, the hard segments that form the physical cross-links are responsible for maintaining the original shape. The reduction in shape recovery following an increase in the number of cycles indicates that there are some hard segments chains that are not well oriented after going through a repetitive deformation cycle ([Fig. 15](#)) ([Jana et al., 2008](#)). This results in a reduction of elastic recoil and the formation of higher strain residues ([Kim et al., 1996](#)). Therefore, lower shape recovery is obtained in the next recovery cycle. [Raja et al. \(2013\)](#) also found similar observations in their study on CNT -filled PU/poly(lactic acid) composites. According to them, the reduction in the shape

**Fig. 13** Shape memory behaviour of SMPU/MWCNT (a) temporary shape after load removal, and (b) permanent shape.

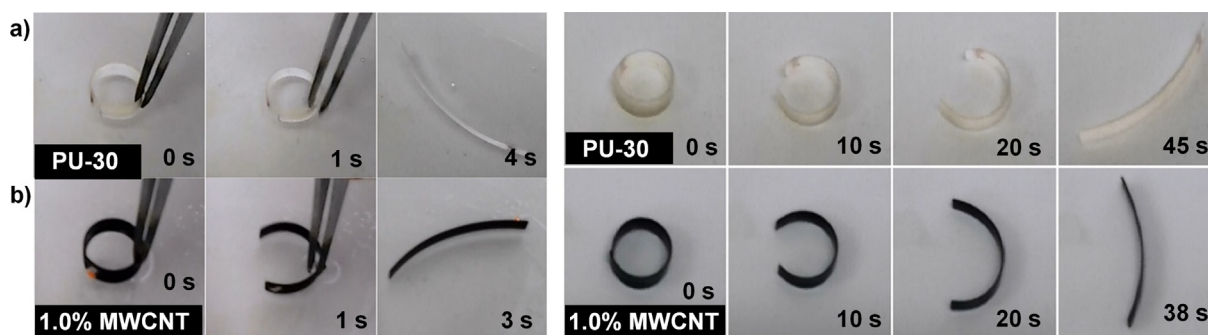


Fig. 14 Changes during shape recovery of PU-30 and PU-30 nanocomposites a) in hot water and b) on a hotplate at 50 °C.

Table 7 Shape memory cycle of pure SMPU and PU-30 nanocomposites.

	Cycle 1		Cycle 2		Cycle 3		Cycle 4	
	SF	SR	SF	SR	SF	SR	SF	SR
PU-0	100	100	100	95.0	100	94.4	100	91.7
PU-10	100	100	100	97.4	100	95.0	100	92.2
PU-20	100	100	100	98.9	100	97.4	100	95.0
PU-30	94.4	100	96.7	97.4	100	97.2	100	96.7
PU-40	84.4	100	92.2	93.9	94.4	91.7	96.7	90.0
PU-30								
0.5% MWCNT	99.6	100	100	96.7	100	96.7	100	94.4
1.0% MWCNT	99.3	100	100	96.7	100	96.1	100	96.1
1.5% MWCNT	99.3	100	100	96.1	100	95.6	100	95.0
2.0% MWCNT	97.8	100	98.9	94.4	100	92.2	100	91.7

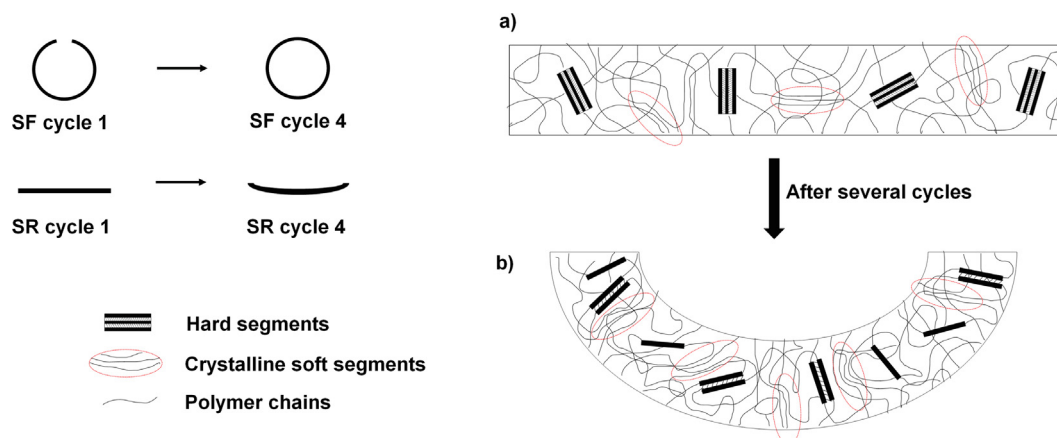


Fig. 15 Possible mechanism for PU-30 a) in the first cycle and b) cycle 4.

recovery obtained is due to the formation of more crystals following the increase in the orientation of the molecular segments in the direction of external forces during repeated deformations. The presence of residual strain found at the beginning of Cycle 2 indicates that irreversible strain is the dominant factor influencing the shape memory effect in this study. Based on Cycle 4, PU-30 nanocomposites filled with MWCNT shows lower shape recovery values compared to PU-30 without filler. This observation suggests that the pres-

ence of MWCNT filler leads to the formation of more unoriented rigid segment structures after several repeated deformations.

4. Conclusions

This paper examined the influence of MWCNT on the soft segment crystallinity, thermal stability, tensile and shape memory behaviour of SMPU nanocomposites. The use of MWCNT, which possessed high

thermal stability properties as filler has improved the thermal properties of the resulting nanocomposites. The degradation temperature of urethane linkage into polyol and isocyanate components has increased by ~60 °C for SMPU nanocomposite compared to the pristine SMPU. In general, the mechanical properties of SMPU nanocomposite are enhanced through the introduction of a lower amount of MWCNT. However, with increasing the amount of MWCNT, the breaking strength and strain at break are compromised. The addition of MWCNT in the PU matrix has enhanced the PCL soft segment crystallisation. MWCNT acts as a nucleating agent, which increases the degree of PCL crystallinity. The percentage of crystallinity between 19 and 24% provides 100% shape fixity for PU-0, PU-10 and PU-20 samples, whereas the shape fixity for PU-30 and PU-40 increased with increasing MWCNT content consistent with the increase of PCL crystallinity. On the other hand, all the samples show excellent shape recovery, which is 100%. The addition of MWCNT has reduced the shape recovery time, and during the shape memory cycle, the SF value increases while the SR value decreases with the increase of the shape memory cycle. Based on the analyses, the resulting SMPU nanocomposites exhibit promising properties and are suitable as smart materials for various industrial applications.

Acknowledgements

This work was supported by the Research University Grant of Universiti Sains Malaysia with a Grant No. 1001/PBAHAN/8014154.

References

- Abolins, A., Yakushin, V., Vilsone, D., 2018. Properties of polyurethane coatings based on linseed oil phosphate ester polyol. *J. Renew. Mater.* 6 (7), 737–745.
- Ahmad Zubir, S., Mat Saad, N., Harun, F.W., Ali, E.S., Ahmad, S., 2018. Incorporation of palm oil polyol in shape memory polyurethane: Implication for development of cardiovascular stent. *Polym. Adv. Technol.* 29 (12), 2926–2935.
- Akindoyo, J.O., Beg, M.D.H., Ghazali, S., Islam, M.R., Jeyaratnam, N., Yuvaraj, A.R., 2016. Polyurethane types, synthesis and applications – a review. *RSC Adv.* 6 (115), 114453–114482.
- Asefnejad, A., Khorasani, M.T., Behnamghader, A., Farsadzadeh, B., Bonakdar, S., 2011. Manufacturing of biodegradable polyurethane scaffolds based on polycaprolactone using a phase separation method: physical properties and in vitro assay. *Int. J. Nanomed.* 6, 2375–2384.
- Asensio, M., Costa, V., Nohales, A., Bianchi, O., Gómez, C.M., 2019. Tunable structure and properties of segmented thermoplastic polyurethanes as a function of flexible segment. *Polymers.* 11, 1910.
- Babaie, A., Rezaei, M., Sofla, R.L.M., 2019. Investigation of the effects of polycaprolactone molecular weight and graphene content on crystallinity, mechanical properties and shape memory behavior of polyurethane / graphene nanocomposites. *J. Mech. Behav. Biomed. Mater.* 96, 53–68.
- Błażek, K., Kasprzyk, P., Datta, J., 2020. Diamine derivatives of dimerized fatty acids and bio-based polyether polyol as sustainable platforms for the synthesis of non-isocyanate polyurethanes. *Polymer.* 205.
- Cai, Y., Jiang, J.S., Liu, Z.W., Zeng, Y., Zhang, W.G., 2013. Magnetically-sensitive shape memory polyurethane composites crosslinked with multi-walled carbon nanotubes. *Compos.: Part A.* 53, 16–23.
- Castilla-Cortázar, I., Vidaurre, A., Marí, B., Campillo-Fernández, A. J., 2019. Morphology, Crystallinity, and Molecular Weight of Poly (ε-caprolactone)/Graphene Oxide Hybrids. *Polymers.* 11 (7), 1099.
- Chakoli, A.N., Wan, J., Feng, J.T., Amirian, M., Sui, J.H., Cai, W., 2009. Functionalization of multiwalled carbon nanotubes for reinforcing of poly(L-lactide-co-ε-caprolactone) biodegradable copolymers. *Appl. Surf. Sci.* 256, 170–177.
- Chen, J., Zhang, Z.-X., Huang, W.-B., Yang, J.-H., Wang, Y., Zhou, Z.-W., Zhang, J.-H., 2015. Carbon nanotube network structure induced strain sensitivity and shape memory behavior changes of thermoplastic polyurethane. *Mater. Des.* 69, 105–113.
- Deka, H., Karak, N., Kalita, R.D., Buragohain, A.K., 2010. Biocompatible hyperbranched polyurethane/multi-walled carbon nanotube composites as shape memory materials. *Carbon.* 48 (7), 2013–2022.
- Díaz, E., Aresti, J., León, J., 2021. Evaluation of physicochemical and mechanical properties with the in vitro degradation of PCL/nHA/MWCNT composite scaffolds. *J. Reinf. Plast. Compos.* 40 (3–4), 134–142.
- El Mahdi, A., M'sahel, M., Medimagh, R., 2017. Catalyst-Free Ring Opening Synthesis of Biodegradable Poly(ester-urethane)s Using Isosorbide Bio-Based Initiator. *Macromol. Chem. Phys.* 218, 1700077.
- Ghahremani, P., Mostafatabar, A.H., Bahlakeh, G., Ramezanzadeh, B., 2022. Rational design of a novel multi-functional carbon-based nano-carrier based on multi-walled-CNT-oxide/poly-dopamine/chitosan for epoxy composite with robust pH-sensitive active anti-corrosion properties. *Carbon.* 189, 113–141.
- Gómez-Rojo, R., Alameda, L., Rodríguez, Á., Calderon, V., Gutiérrez-González, S., 2019. Characterization of Polyurethane Foam Waste for Reuse in Eco-Efficient Building Materials. *Polymers.* 11, 359.
- Gunes, I.S., Cao, F., Jana, S.C., 2008. Evaluation of nanoparticulate fillers for development of shape memory polyurethane nanocomposites. *Polymer.* 49, 2223–2234.
- Hajjalizadeh, S., Barikani, M., Bellah, S.M., 2017. Synthesis and characterization of multiwall carbon nanotube/waterborne polyurethane nanocomposites. *Polym. Int.* 66, 1074–1083.
- Haryńska, A., Kucinska-Lipka, J., Sulowska, A., Gubanska, I., Kostrzewa, M., Janik, H., 2019. Medical-Grade PCL Based Polyurethane System for FDM 3D Printing—Characterization and Fabrication. *Materials.* 12, 887.
- Hassanzadeh-Aghdam, M.K., Ansari, R., Mahmoodi, M.J., 2019. Thermo-mechanical properties of shape memory polymer nanocomposites reinforced by carbon nanotubes. *Mech. Mater.* 129 (May), 80–98.
- Huang, J., Zhang, J., Zhu, G., Yu, X., Hu, Y., Shang, Q., Chen, J., Hu, L., Zhou, Y., Liu, C., 2021. Self-healing, high-performance, and high-biobased-content UV-curable coatings derived from rubber seed oil and itaconic acid. *Prog. Org. Coat.* 159, 106391.
- Jana, R.N., Yoo, H.J., Cho, J.W., 2008. Synthesis and properties of shape memory polyurethane nanocomposites reinforced with poly (ε-caprolactone)-grafted carbon nanotubes. *Fibers Polym.* 9 (3), 247–254.
- Javaid, M.A., Zia, K.M., Iqbal, A., Ahmad, S., Akram, N., Liu, X., Nawaz, H., Khosa, M.K., Awais, M., 2020. Utilization of Waxy Corn Starch as an Efficient Chain Extender for the Preparation of Polyurethane Elastomers. *Int. J. Biol. Macromol.* 148, 415–423.
- Jeong, F.H., Yang, J., Lee, H.S., Seo, S.W., Baik, D.H., Kim, J., Youk, J.H., 2008. Effective preparation and characterization of montmorillonite/poly(ε-caprolactone)-based polyurethane nanocomposites. *J. Appl. Polym. Sci.* 49, 2223–2234.
- Jiang, L., Ren, Z., Zhao, W., Liu, W., Liu, H., Zhu, C., 2018. Synthesis and structure/properties characterizations of four polyurethane model hard segments. *R. Soc. Open Sci.* 5.
- Jin, S.H., Park, Y.B., Yoon, K.H., 2007. Rheological and mechanical properties of surface modified multi-walled carbonnanotube-filled PET composite. *Compos. Sci. Technol.* 67, 3434–3441.

- Joseph, J., Patel, R.M., Wenham, A., Smith, J.R., 2018. Biomedical applications of polyurethane materials and coatings. *Trans. Inst. Met. Finish.* 96 (3), 121–129.
- Karak, N., 2017. Biobased Hyperbranched Polyurethane. *Biobased Smart Polyurethane Nanocomposites: From Synthesis to Applications*, 1–40.
- Kim, B.K., Lee, S.Y., Xu, M., 1996. Polyurethane having shape memory effect. *Polymer*. 37 (26), 5781–5793.
- Kumar, B., Noor, N., Thakur, S., Pan, N., Narayana, H., Yan, S.C., Wang, F., Shah, P., 2019. Shape Memory Polyurethane-Based Smart Polymer Substrates for Physiologically Responsive. Dynamic Pressure (Re) Distribution. *ACS Omega*. 4 (13), 15348–15358.
- Kumar, D., Jindal, P., 2019. Effect of multi-walled carbon nanotubes on thermal stability of polyurethane nanocomposites. *Mater. Res. Express*. 6, (10) 105336.
- Mahapatra, S.S., Yadav, S.K., Yoo, H.J., Cho, J.W., Park, J.S., 2013. Highly branched polyurethane: Synthesis, characterization and effects of branching on dispersion of carbon nanotubes. *Compos.: Part B*. 45, 165–171.
- Malani, R.S., Malshe, V.C., Thorat, B.N., 2022. Polyols and polyurethanes from renewable sources: past, present and future—part I: vegetable oils and lignocellulosic biomass. *J. Coat. Technol. Res.* 19, 201–222.
- Mat Saad, N., Mohd Salleh, N., Abdullah, T.K., Ahmad Zubir, S., 2021. Influence of prepolymer reaction time in the fabrication of palm kernel oil polyol based shape memory polyurethane. *J. Appl. Polym. Sci.* 2021, e52109.
- Meng, Q., Hu, J., Mondal, S., 2009. A review of shape memory polymer composites and blends. *J. Membr. Sci.* 319, 102–110.
- Mondal, S., Hu, J., 2006. Shape memory studies of functionalized MWNT-reinforced polyurethane copolymers. *Iran. Polym. J.* 15 (2), 135–142.
- Oushabi, A., Sair, S., Abboud, Y., Tanane, A., Bouari, E., 2017. An experimental investigation on morphological, mechanical and thermal properties of date palm particles reinforced polyurethane composites as new ecological insulating materials in building. *Case Stud. Constr. Mater.* 7, 128–137.
- Pillai, P.K.S., Li, S., Bouzidi, L., Narine, S.S., 2016. Metathesized palm oil polyol for the preparation of improved bio-based rigid and flexible polyurethane foams. *Ind. Crops Prod.* 83, 568–576.
- Poudel, Y.R., Li, W., 2018. Synthesis, properties, and applications of carbon nanotubes filled with foreign materials: a review. *Mater. Today Phys.* 7, 7–34.
- Qiu, H., Hölken, I., Gapeeva, A., Filiz, V., Adelung, R., Baum, M., 2018. Development and Characterization of Mechanically Durable Silicone-Polythiourethane Composites Modified with Tetrapodal Shaped ZnO Particles for the Potential Application as Fouling-Release Coating in the Marine Sector. *Materials (basel)* 11 (12), 2413.
- Rahman, M.M., Rabbani, M.M., Saha, J.K., 2018. Polyurethane and Its Derivatives. In: Jafar, Mazumder M., Sheardown, H., Al-Ahmed, A. (Eds.), *Functional Polymers*. Polym. Polym. Compos.: A Reference Series. Springer, Cham.
- Raja, M., Ryu, S.H., Shanmugaraj, A.M., 2013. Thermal, mechanical and electroactive shape memory properties of polyurethane (PU)/poly (lactic acid) (PLA)/CNT nanocomposites. *Eur. Polym. J.* 49 (11), 3492–3500.
- Rana, S., Karak, N., Cho, J.W., Kim, Y.H., 2008. Enhanced dispersion of carbon nanotubes in hyperbranched polyurethane and properties of nanocomposites. *Nanotechnology*. 19, 495707.
- Reghunadhan, A., Jibin, K.P., Kaliyathan, A.V., Velayudhan, P., Strankowski, M., Thomas, S., 2021. Shape Memory Materials from Rubbers. *Materials (basel)* 14 (23), 7216.
- Richardson, T.B., Mosiewicki, M.A., Uzunpinar, C., Marcovich, N. E., Aranguren, M.I., Kilinc-Balci, F.R.M.B., Auad, M.L., 2011. Study of nanoreinforced shape memory polymers processed by casting and extrusion. *Polym. Compos.* 32 (3), 455–463.
- Sahebi Joubari, I., Haddadi-Asl, V., Mirhosseini, M.M., 2018. Formulation of micro-phase separation kinetics of polyurethane nanocomposites. *Polym. Adv. Technol.* 29 (12), 2909–2916.
- Sahoo, N.G., Jung, Y.C., Yoo, H.J., Cho, J.W., 2007. Influence of carbon nanotubes and polypyrrole on the thermal, mechanical and electroactive shape-memory properties of polyurethane nanocomposites. *Compos. Sci. Technol.* 67, 1920–1929.
- Sánchez-Urbano, F., Paz-Gómez, G., Rodríguez-Alabanda, Ó., Romero, P.E., Cabrerizo-Vilchez, M., Rodríguez-Valverde, M.Á., Guerrero-Vaca, G., 2018. Non-Stick Coatings in Aluminium Molds for the Production of Polyurethane Foam. *Coatings*. 8 (9), 301.
- Senin, R.M., Ion, I., Ion, A.C., 2018. A Sorption Study of Bisphenol A in Aqueous Solutions on Pristine and Oxidized Multi-Walled Carbon Nanotubes. *Pol. J. Environ. Stud.* 27 (5), 2245–2257.
- Shirole, A., Perotto, C.U., Balog, S., Weder, C., 2018. Tailoring the Shape Memory Properties of Segmented Poly(ester urethanes) via Blending. *ACS Appl. Mater. Interfaces*. 10 (29), 24829–24839.
- Su, X., Wang, R., Li, X., Araby, S., Kuan, H., Naeem, M., Ma, J., 2021. A comparative study of polymer nanocomposites containing multi-walled carbon nanotubes and graphene nanoplatelets. *Nano Mater. Sci.*
- Tijing, L.D., Park, C.H., Choi, W.L., Ruelo, M.T.G., Amarjargal, A., Pant, H.R., Im, I.T., Kim, C.S., 2013. Characterization and mechanical performance comparison of multiwalled carbon nanotube/polyurethane composites fabricated by electrospinning and solution casting. *Compos.: Part B*. 44, 613–619.
- Trinh, N.H., Jaafar, M., Viet, C.X., Zubir, S.A., 2020. Palm kernel oil polyol based shape memory polyurethane: effect of polycaprolactone and polyethylene glycol as soft segment. *Mater. Res. Express*. 7 (2), 25704.
- Trujillo, M., Arnal, M.L., Müller, A.J., Mujica, M.A., Urbina De Navarro, C., Ruelle, B., Dubois, P., 2012. Supernucleation and crystallization regime change provoked by MWNT addition to poly(ϵ -caprolactone). *Polymer*. 53 (3), 832–841.
- Wang, X., Jian, W., Lu, H., Lau, D., Fu, Y.Q., 2021a. Selective entanglement coupling of nanoparticles in polymer nanocomposite with high shape recovery stress. *Compos. Sci. Technol.* 207 (November), 108728.
- Wang, Z., Li, X., Pösel, E., Eling, B., Wang, Z., 2021b. Melting behavior of polymorphic MDI/BD-block TPU investigated by using in-situ SAXS/WAXS and FTIR techniques. Hydrogen bonding formation causing the inhomogeneous melt. *Polym. Test.* 96, 107065.
- Yadav, S.K., Mahapatra, S.S., Cho, J.W., 2012. Synthesis of mechanically robust antimicrobial nanocomposites by click coupling of hyperbranched polyurethane and carbon nanotubes. *Polymer*. 53, 2023–2031.
- Yang, D., Tian, D., Xue, C., Gao, F., Liu, Y., Li, H., Bao, Y., Liang, J., Zhao, Z., Qiu, J., 2018. Tuned Fabrication of the Aligned and Opened CNT Membrane with Exceptionally High Permeability and Selectivity for Bioalcohol Recovery. *Nano Lett.* 18 (10), 6150–6156.
- Yap, S.Y., Yusrizal, A.A., Abdullah, T.K., Ahmad Zubir, S., 2021. Heat-induced shape memory polyurethane with inclusion of palm kernel oil. *Malays. J. Microsc.* 17 (2), 66–77.
- Yazdi, M.A., Haddadi Asl, V., Pourmohammadi, M.H., Roghani-Mamaqani, H., 2019. Mechanical properties, crystallinity, and self-nucleation of carbon nanotube-polyurethane nanocomposites. *Polym. Test.* 79, 106011.
- Zhang, J., Huang, J., Zhu, G., Yu, X., Cheng, J., Liu, Z., Hu, Y., Shang, Q., Liu, C., Hu, L., Zhou, Y., 2021. Self-healing, recyclable, and removable UV-curable coatings derived from tung oil and malic acid. *Green Chem.* 23, 5875–5886.
- Zhang, J., Zhang, C., Song, F., Shang, Q., Hu, Y., Jia, P., Liu, C., Hu, L., Zhu, G., Huang, J., Zhou, Y., 2022. Castor-oil-based, robust, self-healing, shape memory, and recyclable polymers enabled by dynamic hindered urea bonds and hydrogen bonds. *Chem. Eng. J.* 429, 131848.